VIETNAM ACADEMY OF SCIENCE AND TECHNOLOGY

GRADUATE UNIVERSITY OF SCIENCE AND TECHNOLOGY

Nguyen Tuan Anh

FABRICATION OF TITANIUM DIOXIT AND PORPHYRIN-BASED NANOMATERIALS AND THEIR APPLICAITON AS PHOTOCATALYST FOR PHOTODEGRADATION OF RHODAMINE B IN AQUEOUS MEDIA

PhD THESIS ABSTRACT IN INORGANIC CHEMISTRY

Mã số: 9 44 01 13

Ha Noi - 2024

This dissertation was completed at: Graduate University of Science and Technology, Vietnam Academy of Science and Technology

Supervisors:

1. Supervisor 1: *Prof. Dr. Tran Dai Lam*
2. Supervisor 2: *Assoc.Prof.Dr. La Duc Duong*

Referee 1:……..

Referee 2: ……..

Referee 3: ……..

The dissertation is defended before the Academy-level Doctoral Dissertation Evaluation Council meeting at Graduate University of Sciene and Technology, Vietnam Academy of Science and Technology at … giờ …', date … month … year 2024

The dissertation could be found at:
1. Library of Gradudate University of Sciene and Technology
2. National Library of Vietnam

INTRODUCITON

1. The urgencey of the dissertation

TiO_2 has long been commonly used as a photocatalyst in the treatment of organic pollutants in water and air since the 1970s. TiO_2 is often modified with metals, metal oxides, or carbon-structured materials to overcome its disadvantages and improve its photocatalytic performance.

Porphyrins play an important role in biological processes, functioning as catalysts and light absorbers in photosynthesis. Several porphyrin-based nanomaterials have been reported to exhibit high photocatalytic activity in the treatment of organic compounds and dyes. The combination of nanomaterials such as TiO_2 and porphyrin nanostructures has significantly improved photocatalytic properties due to enhanced light absorption and improved charge separation efficiency.

Therefore, the aforementioned questions arise to better understand the photocatalytic mechanisms of porphyrin nanostructured materials, which not only address questions about the process of biological energy replenishment occurring in nature but also create a new, efficient line of photocatalytic materials for environmental treatment.

Based on the practical significance mentioned above, the candidate has chosen and conducted the study titled " Fabrication of titanium dioxit and porphyrin-based nanomaterials and their applicaiton as photocatalyst for photodegradation of rhodamine b in aqueous media"

2. Research objectives of the dissertation:

- Synthesize porphyrin nanomaterials using the self-assembly method, TiO_2 nanomaterials, and hybrid materials based on TiO_2 and porphyrin nanomaterials.

- Investigate the photocatalytic activity in the degradation of Rhodamine B in aqueous environments using these materials and propose the catalytic mechanism of the synthesized materials.

3. The main research contents of the dissertation

- Study the synthesis of nanostructured materials from new porphyrin derivatives (TCPP, TTPAP, and TTOP) using the self-assembly method, capable of being used as photocatalytic materials for the degradation of Rhodamine B in aqueous environments.

- Investigate the synthesis of hybrid nano TiO_2/TCPP materials using the self-assembly method, exhibiting high photocatalytic activity for the degradation of Rhodamine B in water under simulated sunlight.

- Study the synthesis of hybrid nano graphene/Fe_2O_3-TiO_2/TCPP materials using the self-assembly method, showing effective photocatalytic activity for the degradation of Rhodamine B in water under simulated sunlight.

Chapter 1. OVERVIEW

1.1. Introduciton of photocatalysis

1.1.1. Mechanism and conditions of photocatalytic reaction

Photocatalysis is a process that involves utilizing solar light energy for chemical reactions, including reactions facilitated by light and semiconductors.

1.1.2. Factors Influencing Photocatalytic Activity

1.1.2.1. Influence of dye concentration

1.1.2.2. Influence of catalyst amount

1.1.2.3. Influence of pH

1.1.2.4. Morphology and surface area of the photocatalyst

1.1.2.5. Influence of reaction temperature

1.1.2.6. Influence of inorganic ions

1.1.2.7. Influence of light intensity and irradiation time

1.1.3. Photocatalytic Materials

1.1.3.1. Composite materials based on graphene

1.1.3.2. Binary photocatalysts based on oxides

1.1.3.3. Binary photocatalysts based on transition metals

1.1.3.4. Ternary photocatalytic materials

1.1.3.5. Polymeric photocatalytic materials

1.2. TiO_2 materials

1.2.1. Definition and general characteristics of TiO_2

TiO_2 is a bright white solid commonly used primarily as a pigment in a wide range of popular products today. TiO_2 exists in four different polymorphs, including rutile, brookite, anatase, and amorphous forms.

1.2.2. Photocatalytic behaviour of TiO_2

A material exhibits photocatalytic activity when: (1) It can absorb energy from light sources; (2) It has an appropriate band gap energy to absorb light and generate electron-hole pairs in the visible to ultraviolet spectrum.

1.2.3. Functionalization of TiO_2

1.2.3.1. Doping with metals

1.2.3.2. Doping with non-metals

1.2.3.3. Functionalization with carbon-based nanomaterials

1.2.3.4. Size modification of TiO_2 nanoparticles

1.3. Introduction of porphyrin

Porphyrins participate in processes involving gas transport, catalysis, and light absorption in many animal and plant species. Chlorophyll is a crucial biological molecule comprising tetra-pyrrolic units, particularly chlorin and porphyrin structures.

1.3.1. Fabrication of porphyrin nanostructures via self-assembly

1.3.1.1. Ion self-assembly

1.3.1.2. Coordination polymerization method

Nano porphyrins formed via self-assembly sequences can be effectively utilized in various photocatalytic applications for environmental treatment.

Rhodamine B is a widely used and toxic dye, commonly employed in industries such as textile dyeing, paper production, paints, plastics, pharmaceuticals, and more. Even at low concentrations, Rhodamine B can have serious impacts on ecological environments and human health.

Porphyrin nanostructures have been extensively studied for their photocatalytic properties in the visible light region to remove dyes and organic compounds from water environments. Self-assembled porphyrins are used as photocatalysts for environmental remediation in the form of free nano porphyrins or hybrid materials based on porphyrins.

In Vietnam, photocatalysis has attracted significant attention from scientists with numerous publications. Research efforts aim to discover methods to enhance photocatalytic efficiency.

Chapter 2
EXPERIMENTAL SECTION

Dissolve 8 mg of TCPP in a vial containing 1 mL of 0.2 M NaOH solution, referred to as solution A. Solution B consists of 0.01 M HCl. Slowly add solution B

to solution A until the pH of the mixture reaches approximately 7 under stirring at room temperature, in the dark, for about 1 hour. The precipitate obtained is filtered, washed with distilled water, and dried for further characterization.

2.2.1.2. Synthesis of porphyrin nanostructures from TTPAP molecules

Dissolve 8 mg of TTPAP in a vial containing 8 mL of THF solvent. Stir the mixture at room temperature in the dark for 1 hour. Then, sequentially add portions of water with varying volume ratios (0–100%) into the porphyrin solution until precipitation occurs. Finally, filter the precipitate, wash it with distilled water, and dry it for characterization of its properties.

2.2.1.3. Synthesis of porphyrin nanostructures from TTOP molecules

Dissolve 40 mg of TTOP monomer in 40 mL of THF solvent. Stir the mixture at room temperature in the dark for 1 hour. Sequentially add portions of water with varying volume ratios (from 10% to 90%) into the porphyrin solution, causing precipitation to form. Filter the precipitate, wash it multiple times with distilled water, and dry it to determine its properties.

2.2.2. Synthesis of TiO_2/TCPP

2.2.2.1. Synthesis of TiO_2 nanomaterials

Add 3 mL of $TiCl_4$ dropwise into 30 mL of ethanol at room temperature, resulting in a light-yellow solution. Let the solution stand in the dark for 2 days to form a sol-gel. Subsequently, dry the sol-gel solution at 80°C for 6 hours. The dried gel precursor is then calcined at 500°C with a heating rate of 5°C/minute for 3 hours to obtain nano-sized TiO_2 powder.

2.2.2.2. Synthesis of TiO_2/TCPP nanomaterials

First, dissolve 8 mg of TCPP in 1 mL of 0.2 M NaOH solution. Then, disperse 1 mg of TiO_2 powder in this TCPP solution by ultrasonication for 30 minutes (referred to as solution A). Solution B is prepared by dissolving 70 mg of CTAB in 19 mL of 0.01 M HCl solution. Subsequently, add Solution B dropwise into Solution A and vigorously stir at room temperature in the dark for 1 hour.

2.2.3. Synthesis of graphene/Fe_2O_3-TiO_2/TCPP (TFG@TCPP) hybrid material

Synthesis of graphene/Fe_2O_3-TiO_2 (TFG) nanocomposite

First, ilmenite ore (52%) is thoroughly washed with distilled water and dried overnight at 60°C. Next, the ilmenite ore is ball-milled until the particle size is less than 0.149 mm (passing through a 100-mesh sieve). The ilmenite ore is mixed with $KHSO_4$ at a ratio of 1:7 and then calcined at 600°C for 2 hours. The calcined product is dissolved in a 10% H_2SO_4 solution to obtain solution A. 50 ml of ethanol is added to 100 ml of solution A, stirred for 30 minutes to form solution B. 20 mg of Graphene (GNPs) is added to solution B and ultrasonicated with a probe for 30 minutes to achieve a uniformly dispersed mixture. The mixture is transferred into an autoclave and subjected to a hydrothermal reaction at 150°C for 8 hours. Finally, the precipitate is dried in an oven at 80°C and then its properties are evaluated.

Synthesis of graphene/Fe_2O_3-TiO_2/TCPP hybrid material

TCPP (8 mg) and 80 mg of the graphene/Fe_2O_3-TiO_2 nanocomposite mixture are added to a beaker containing 3 ml of 0.2 M NaOH. The mixture is

then ultrasonicated for 30 minutes. Next, 6 ml of 0.01 M HCl is added to the mixture and stirred magnetically for 30 minutes. The mixed solution is kept in the dark for 2 hours, then filtered, washed with distilled water, and dried to obtain a green solid hybrid material for property evaluation.

2.2.4. Study of the photocatalytic properties of the synthesized nanomaterials

Evaluation of the photocatalytic performance of the TCPP, TTPAP, and TTOP nanostructures was conducted on the degradation of RhB in an aqueous environment. Specifically, 0.1 mg of the synthesized material was dispersed in 20 mL of RhB dye with a concentration of 5 ppm. The reaction mixture was kept in the dark for 2 hours to establish adsorption/desorption equilibrium before illumination. After every 30 minutes of illumination, 1.5 mL of the reaction mixture was taken out and centrifuged to remove the photocatalyst. The photocatalytic efficiency of the synthesized samples for the degradation of RhB was evaluated by recording the real-time UV-VIS absorption spectra of RhB at a wavelength of 553 nm.

** The degradation efficiency of RhB is calculated using the formula:*

$$H = \frac{C_0 - C_t}{C_0}.100\%$$

Where: H is the degradation efficiency of RhB (%), and C0C_0C0 and CtC_tCt are the initial concentration of RhB and the concentration at time t in the solution (mg/L), respectively.

2.2.5. Evaluation of the role of free radicals in the photocatalytic degradation of RhB

To evaluate the role of free radicals, the experiment is conducted as follows: prepare solutions containing 10 mM 1,4-benzoquinone (BQ), isopropyl alcohol (IPA), and 10 mM ammonium oxalate (AO), corresponding to the radicals O_2^{-*}, *OH, h^+ và e^-, respectively. Then, add 0.5 mL of each of the BQ, IPA, and AO solutions to glass tubes containing 20 mL of 5 ppm RhB solution with a photocatalyst concentration of 1 g/L. Next, place the tubes in a photoreactor for illumination for a duration of 180 minutes. After the illumination process, remove the catalyst material from the solution and measure the remaining concentration of RhB post-reaction.

2.3. Characterization of materials

2.3.1. Molecular Absorption Spectroscopy (UV-VIS)

2.3.2. Fluorescence Emission Spectroscopy

2.3.3. Scanning Electron Microscopy (SEM)

2.3.4. Energy-Dispersive X-ray Spectroscopy (EDX)

2.3.5. Transmission Electron Microscopy (TEM)

2.3.6. Fourier Transform Infrared Spectroscopy (FTIR)

2.3.7. X-ray Diffraction Spectroscopy (XRD)

2.3.8. X-ray Photoelectron Spectroscopy (XPS)

2.3.9. Total Organic Carbon (TOC) Measurement

Chapter 3
RESULTS AND DISCUSSION

3.1. Synthesis and Characterization of Materials

3.1.1. TCPP porphyrin nanostructure

UV-VIS absorption spectroscopy is used to investigate the optical properties of the sample. The absorption spectrum of the TCPP molecule exhibits a strong Soret band at 412 nm due to π-π* transitions, and four Q bands in the range of 500 to 700 nm. Upon acid neutralization, the intensity of the characteristic Soret band significantly decreases, indicating the formation of a supramolecular assembly (Figure 3.1).

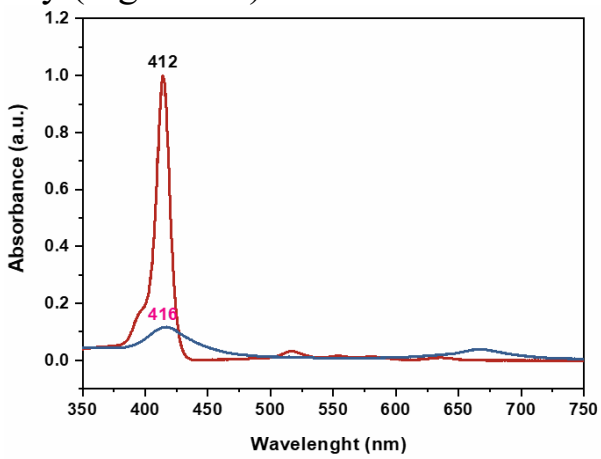

Figure 3.1. UV-VIS spectra of TCPP monomers (black line) and TCPP nanostructured materials after self-assembly (dark red line).

The fluorescence emission (PL) characteristics of TCPP molecules were measured upon excitation of the solution at 400 nm (Figure 3.2). Two characteristic emission peaks were observed at wavelengths 655 nm and 714 nm. Upon neutralization with HCl acid, the emission peaks at 655 nm and 714 nm merged to form a broad peak at 680 nm. The color changes and broadening of the emission peaks are attributed to the self-assembly of TCPP into aggregates.

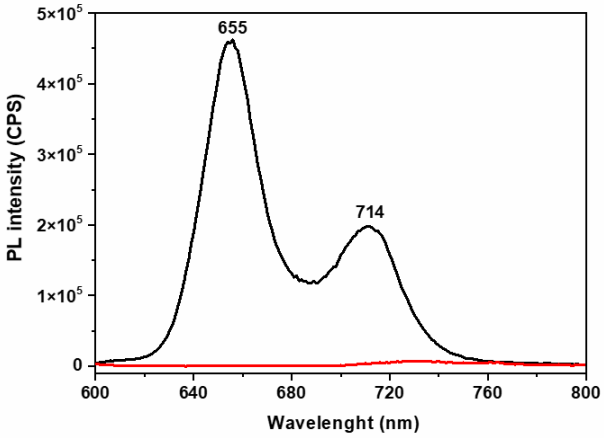

Figure 3.2. Fluorescence emission spectra of TCPP monomers (black line) and TCPP nanostructured materials after self-assembly (red line).

Field-Emission Scanning Electron Microscopy (FE-SEM) was used to describe the self-assembled nanostructures (Figure 3.3 A-B). The SEM images

show that the self-assembled TCPP structures appear as belt-like shapes with lengths of several micrometers and diameters around 20-30 nm.

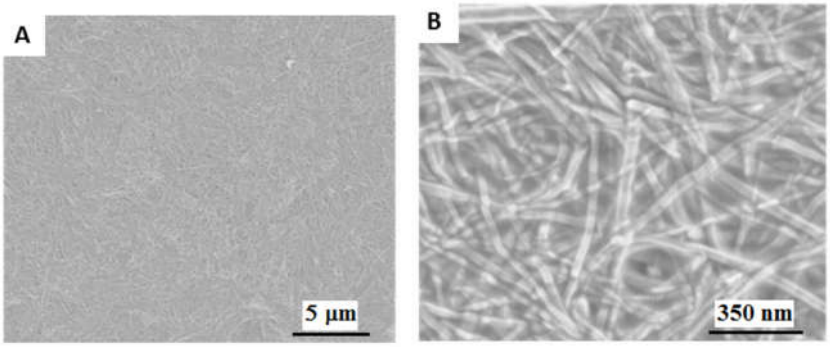

Figure 3.3. SEM images of TCPP nanostructures after self-assembly at various resolutions synthesized using the acid-base self-assembly method.

The TEM images analyzed are shown in Figure 3.4 A-B, clearly demonstrating the formation of TCPP nanostrands with lengths of several micrometers. Consistency between the FESEM and TEM images confirms the well-ordered structure of the self-assembled TCPP nanostrands.

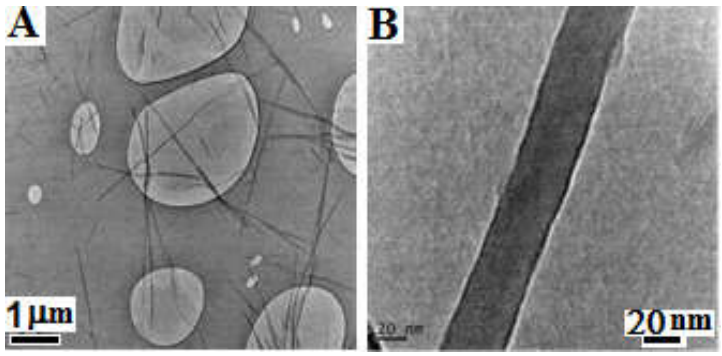

Figure 3.4. TEM images of TCPP nano fibers after self-assembly.

The crystal structure of self-assembled TCPP nanostructures is characterized by X-ray diffraction (XRD) (Figure 3.5). The XRD pattern shows no observable diffraction peaks for TCPP monomers, implying their non-crystalline nature. In contrast, XRD data for self-assembled TCPP reveals two sharp and intense peaks around 31° and 45°. These peaks are attributed to the crystalline structure of TCPP in its synthesized nanostrands.

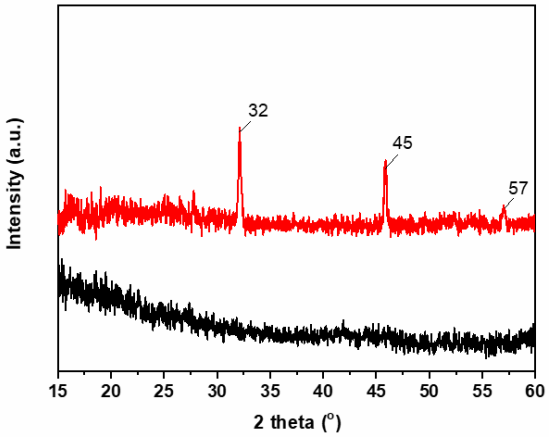

Figure 3.5. X-ray diffraction (XRD) patterns of TCPP monomers and TCPP nanostructured materials after self-assembly.

3.1.2. TTPAP porphyrin nanostructure

UV-VIS spectroscopy was used to study the optical properties of TTPAP monomers and the assemblies formed in THF/H_2O mixtures, as shown in Figure 3.6. Upon adding water to the TTPAP mixture in THF solution, a significant red shift (17 nm) was observed in the absorption spectrum, along with a decrease in intensity compared to the monomer. This significant red shift indicates the formation of J-aggregates within the supramolecular assemblies.

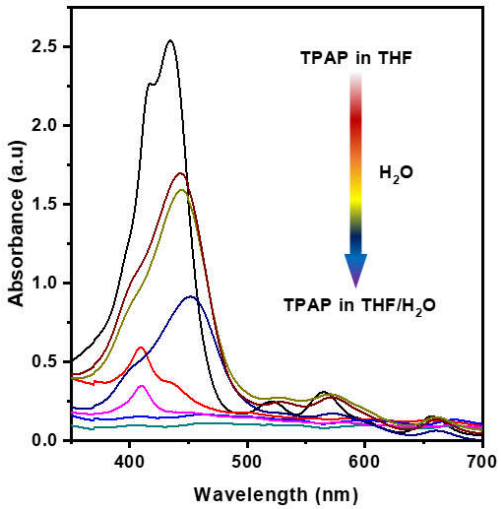

Figure 3.6. UV-VIS spectra of TTPAP monomers in THF with varying ratios of H_2O/THF from 10-90%.

The optical properties of TTPAP as monomers and in aggregated states were investigated by monitoring fluorescence emission after excitation at 435 nm, as shown in Figure 3.7a.

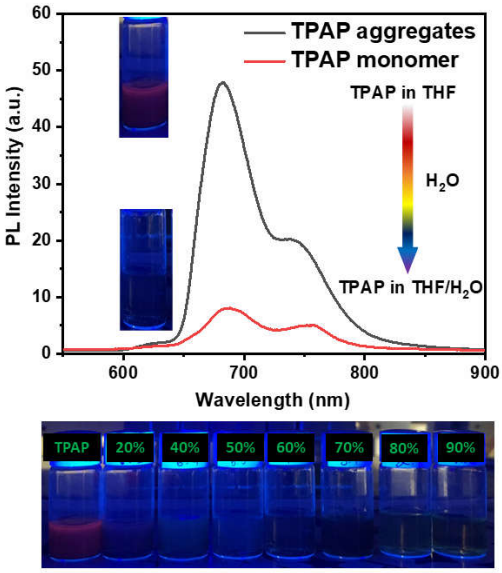

Hình 3.7. (a) Fluorescence emission spectra of TTPAP monomers in neat THF (gray line) and in THF/H_2O mixture with 60% H_2O content (red line); (b) Optical images of TTPAP monomers in neat THF and in THF/H_2O mixture with varying H_2O content under UV light at 435 nm wavelength.

The quenching effects can also be clearly observed visually in the inset of Figures 3.7a and 3.7b. Quenching, or the reduction in fluorescence intensity, results

from π-π stacking and the packing of TTPAP molecules in the aggregation process, which confirms the self-assembly of TTPAP in the THF/H_2O mixture.

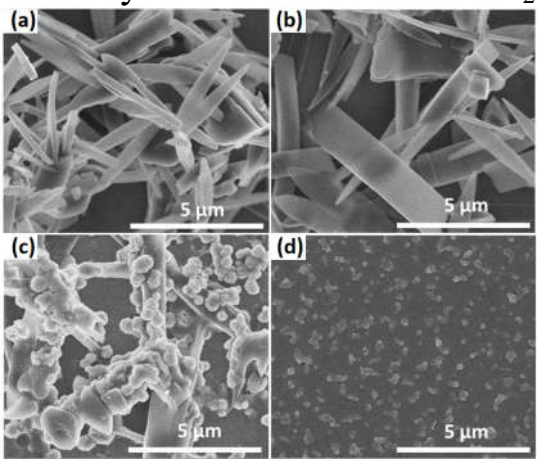

Figure 3.8. SEM images of self-assembled TTPAP in THF/H_2O mixture with varying water content: (a) 50%, (b) 60%, (c) 70%, and (d) 90%.

The self-assembled supramolecular structures of TTPAP in pure THF and THF/H_2O mixtures were examined using SEM (Figure 3.8). It can be observed that without the addition of water, TTPAP molecules do not form structured particles. At a water content of 50%, TTPAP self-assembles into rod-like structures with lengths of about 5 µm and diameters ranging from 0.5–1.5 µm (Figure 3.8a). Increasing the water content to 60% leads to the formation of belt-like structures with diameters around 2 µm and lengths exceeding 10 µm (Figure 3.8b). However, at 70% water content, distinct microstructures with a tendency to aggregate are clearly identified (Figure 3.8c). Furthermore, at 90% water content, only homogeneous particles are observed (Figure 3.8d).

Fourier Transform Infrared Spectroscopy (FTIR) was used to confirm the role of non-covalent interactions of porphyrin molecules in the formation of microstructures through self-assembly. The FTIR spectra of TTPAP monomers and self-assembled TTPAP in THF/H_2O mixtures are shown in Figure 3.9.

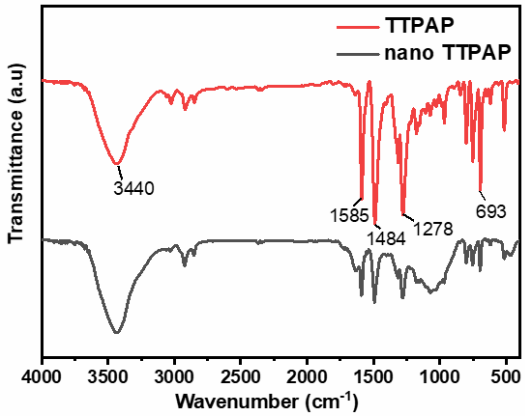

Hình 3.9. Phổ FTIR của đơn phân tử TTPAP và TTPAP tự lắp ráp trong hỗn hợp THF/H_2O

Figure 3.10 shows the X-ray diffraction (XRD) patterns of TTPAP monomers (red line) and TTPAP nanostructures (black line) formed in a THF/H2O mixture with 60% water content. No peaks are observed in the XRD pattern of TTPAP monomers, indicating their amorphous nature in the pure form. The XRD pattern of self-assembled TTPAP in THF/H_2O exhibits sharp

peaks in the range from 15 to 60 degrees, indicating that self-assembled TTPAP has a crystalline structure.

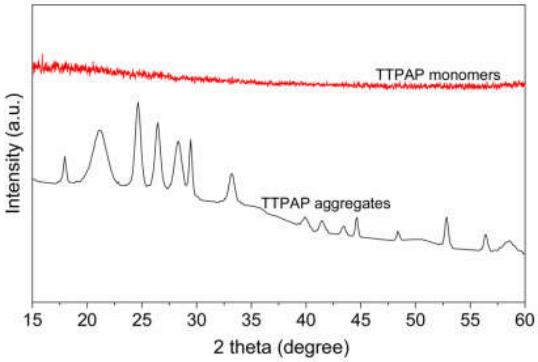

Figure 3.10. X-ray diffraction (XRD) patterns of TTPAP monomers (red line) and crystalline structure of TTPAP in THF/H_2O mixture (60%, v/v) (black line)

3.1.3. TTOP porphyrin nanostructures

The UV-VIS spectrum analysis of TTOP solution shows a strong absorption peak at 420 nm across various ratios of THF/H2O solvent mixtures, as depicted in Figure 3.11.

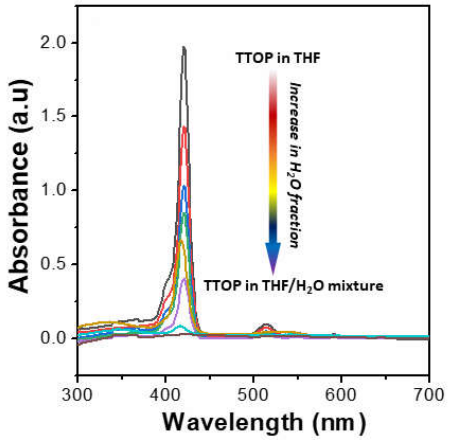

Figure 3.11. UV-VIS spectra of TTOP in THF solvent with varying water content ratios ranging from 20% to 90%.

The fluorescence emission spectra (PL) of TTOP were excited with a laser source at a wavelength of 420 nm to study the influence of water content on the optical properties, as depicted in Figure 3.12.

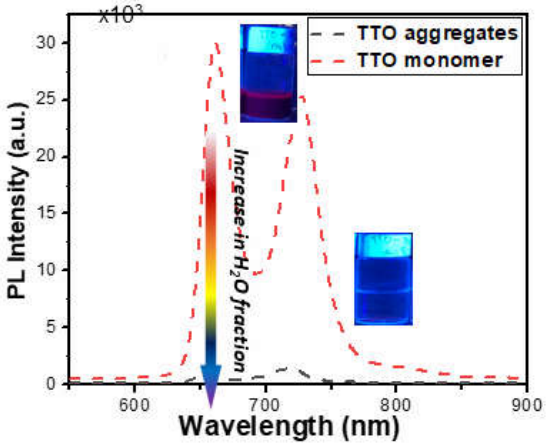

Figure 3.12. PL spectra of TTOP monomer (red line) and self-assembled TTOP (black line) in THF with 90% water content, excited at a wavelength of 420 nm.

The morphological study of self-assembled nano TTOP was conducted using SEM images shown in Figure 3.13. In the image, elongated nanostructures with a diameter of 0.5 nm and lengths around 10 μm can be observed, alongside spherical particles ranging in diameter from 0.5 to 1.2 μm. As the water content increases, the spherical particles almost completely disappear, and instead, plate-like nanostructures appear with lengths similar to the elongated nanorods, approximately 4.5 μm in diameter.

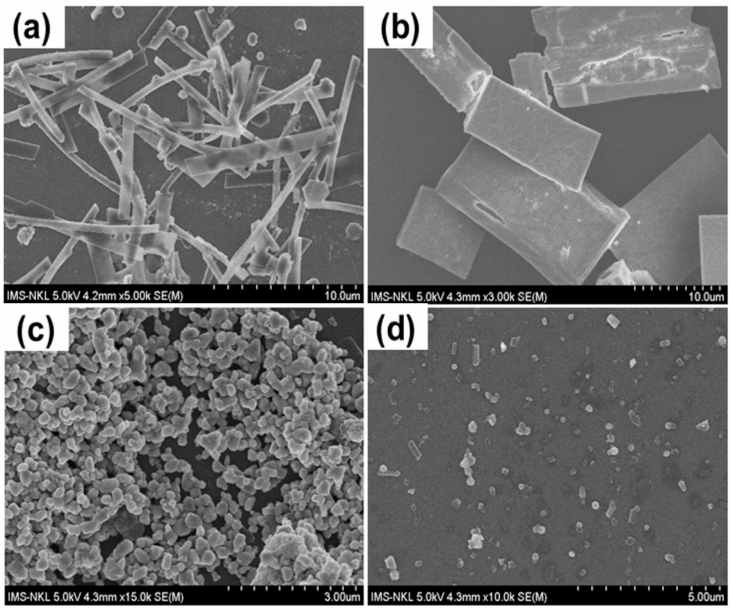

Figure 3.13. SEM images of self-assembled TTOP in THF with varying water ratios: a) 70%, b) 80%, c) 90%, and d) 95%.

3.1.4. TiO_2/TCPP hybrid material

The morphological study of self-assembled nano TiO2 particles, porphyrin TCPP, and the hybrid TiO2/TCPP material was conducted using scanning electron microscopy (SEM), as illustrated in Figure 3.14.

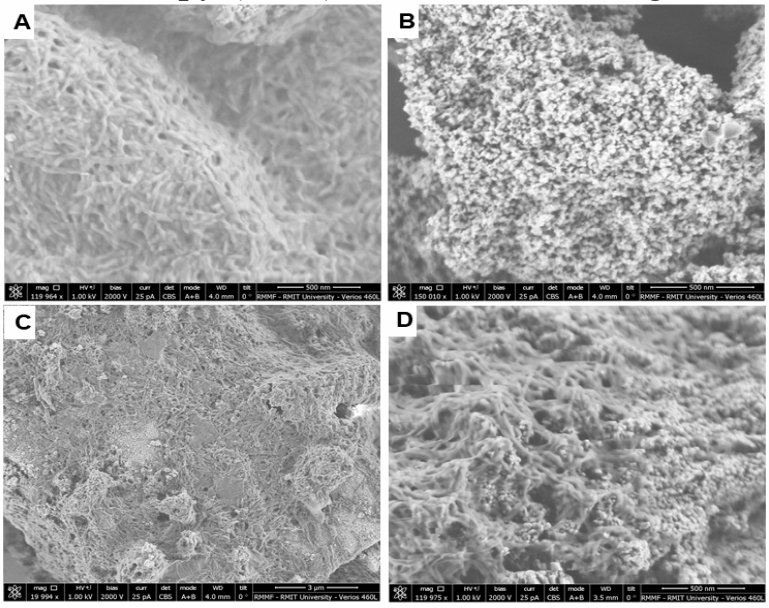

Figure 3.14. SEM images of (A) nano fibers of TCPP, (B) nano particles of TiO_2, and (C, D) hybrid TiO_2/TCPP materials.

Figure 3.15. Transmission electron microscopy (TEM) images of the hybrid TiO_2/TCPP material. The results demonstrate that TiO_2 retains its nanoparticle structure and integrates well into the nano fiber network of TCPP.

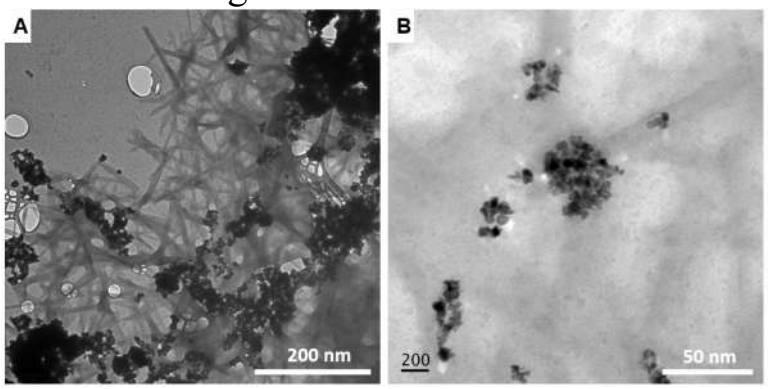

Figure 3.15. TEM image of the hybrid TiO2/TCPP material.

The adsorption of TCPP onto the surface of TiO2 was confirmed using X-ray photoelectron spectroscopy (XPS).

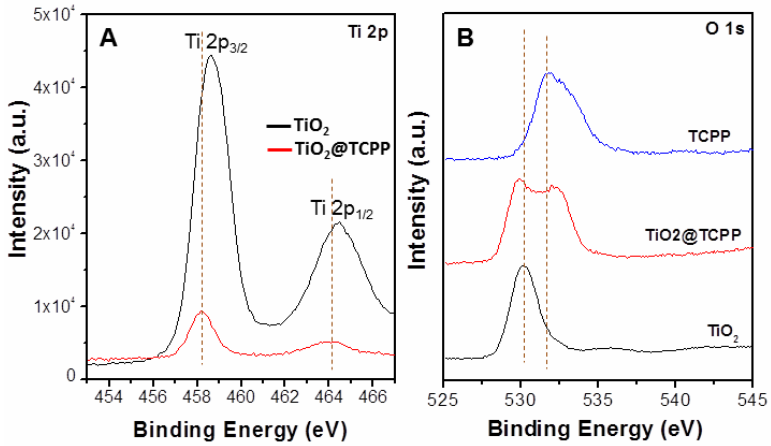

Figure 3.16. XPS spectra showing the binding energy levels of Ti 2p (A) and O 1s (B) in TiO_2, TCPP, and TiO_2/TCPP.

The chemical bonding nature of the materials was analyzed by FT-IR spectroscopy. The FT-IR spectra of TCPP, TiO_2 and TiO_2/TCPP materials are shown in Figure 3.17.

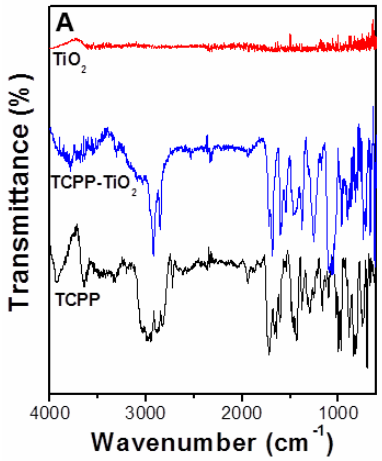

Hình 3.17. Phổ FTIR của TiO_2, TCPP, và TiO_2/TCPP

The crystallinity of TiO_2, TCPP monomers and TiO_2/TCPP hybrids were determined by X-ray diffraction (XRD) as shown in Figure 3.18.

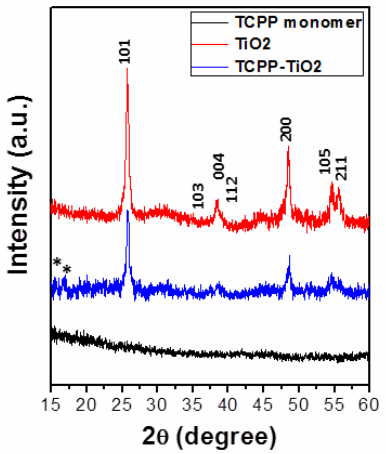

Figure 3.18. XRD patterns of TiO_2, TCPP, and TiO_2/TCPP

The XRD spectrum of TCPP monomers (black line) does not show diffraction peaks, indicating the amorphous nature of TCPP monomers. The position and width of the peak in the X-ray diffraction (XRD) pattern (red line) of TiO_2 particles indicate that the TiO_2 particles are pure anatase nanocrystals.

The optical properties of the samples were studied by UV-VIS spectroscopy and fluorescence emission spectroscopy (Figures 3.19 and 3.20). Figure 3.19 illustrates the UV-VIS spectra of monomeric TCPP molecules and the TiO_2/TCPP nanofiber hybrid.

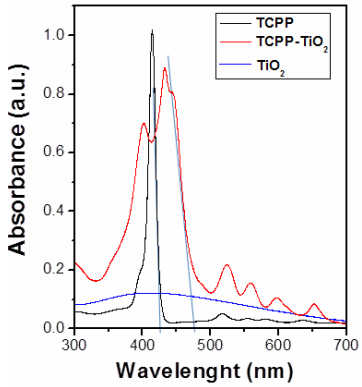

Figure 3.19. UV-VIS spectra of TiO_2, TCPP, and TiO_2/TCPP

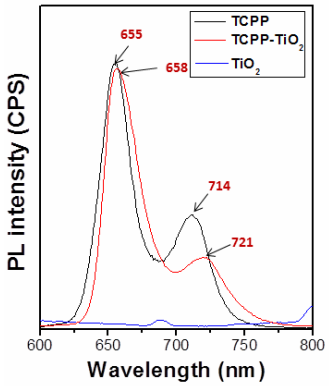

Figure 3.20. Fluorescence emission spectra of TCPP and TiO_2/TCPP excited at 420 nm.

The fluorescence properties of TCPP monomers and TiO_2/TCPP hybrids were investigated by fluorescence emission spectroscopy (Figure 3.20). These redshifts in the emission peaks are likely due to coupling from the spatial assembly of TCPP porphyrin monomers.

3.1.5. Graphene/Fe_2O_3-TiO_2/TCPP (TFG/TCPP) material

The morphology of Fe_2O_3-TiO_2 shows uniform particle size and distribution (Figure 3.21).

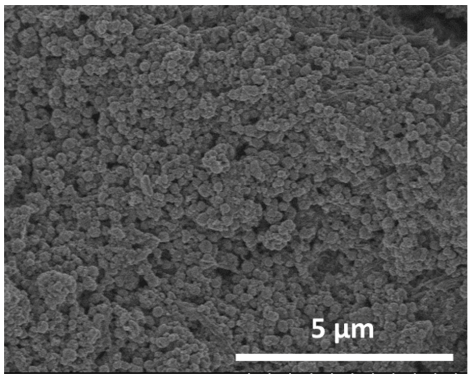

Figure 3.21. SEM image of Fe_2O_3-TiO_2

Figure 3.22 shows the morphology of graphene/Fe_2O_3-TiO_2/TCPP nanohybrid. The porphyrin molecules have self-assembled well into nanofiber structures with diameters of about 100 nm and lengths of several µm.

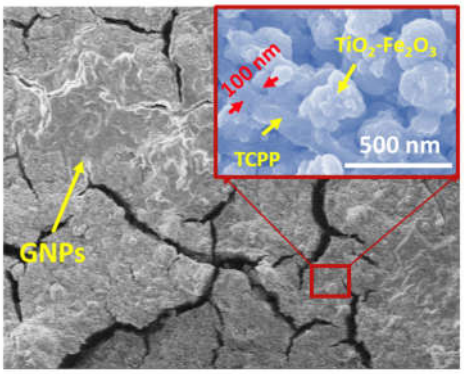

Figure 3.22. SEM (600x magnification) and FE-SEM (inset, 100 thousandx magnification) images of graphene/Fe_2O_3-TiO_2/TCPP nanocomposite

The crystalline phases of graphene/Fe_2O_3-TiO_2 (TFG) and graphene/Fe_2O_3-TiO_2/TCPP were confirmed by XRD (Fig. 3.23), where the characteristic peaks of graphene were not observed due to the low concentration. The XRD pattern of graphene/Fe_2O_3-TiO_2 (black line) shows four prominent diffraction peaks at 2θ of 24.9, 38, 47.9, and 54.9◦, which are attributed to the (101), (004), (200), and (211) crystalline phases of anatase TiO_2, the diffraction peaks of α-Fe_2O_3 phase are also observed in the XRD spectrum.

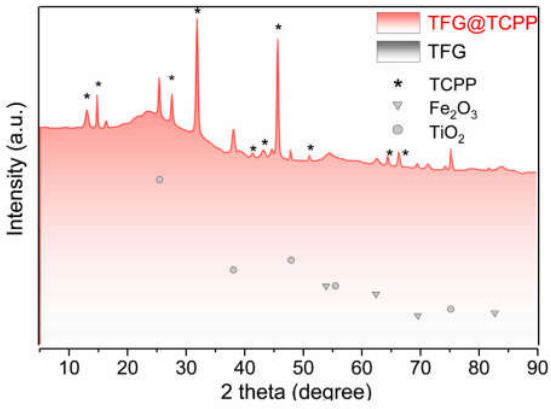

Figure 3.23. X-ray diffraction (XRD) patterns of graphene/Fe_2O_3-TiO_2 (TFG) and graphene/Fe_2O_3-TiO_2/TCPP(TFG/TCPP)

The FT-IR spectrum investigated the functional groups on the surface of graphene/Fe_2O_3-TiO_2/TCPP hybrid materials. Figure 3.24 shows the FTIR spectrum of pure porphyrin and graphene/Fe_2O_3-TiO_2/TCPP hybrid materials.

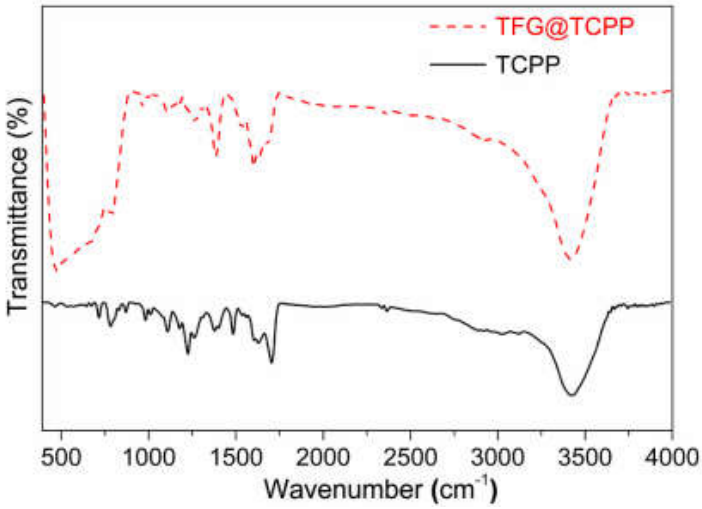

Figure 3.24. FTIR spectra of single porphyrin molecule (TCPP) and graphene/Fe_2O_3-TiO_2/TCPP (TFG/TCPP)

In the UV-VIS spectrum of porphyrin molecules, the absorption peak at 412 nm and four peaks in the range of 500–700 nm are assigned to the Soret band and Q band, respectively, of a porphyrin derivative. These absorption peaks can be attributed to the transition from a1u (π) and a_2u (π) to e^*g (π) states in molecular porphyrin. The absorption peaks at around 400 nm and 670 nm in the UV-VIS spectrum of graphene/Fe_2O_3-TiO_2/TCPP hybrid materials correspond to TiO_2 nanoparticles and graphene/Fe_2O_3 materials, respectively.

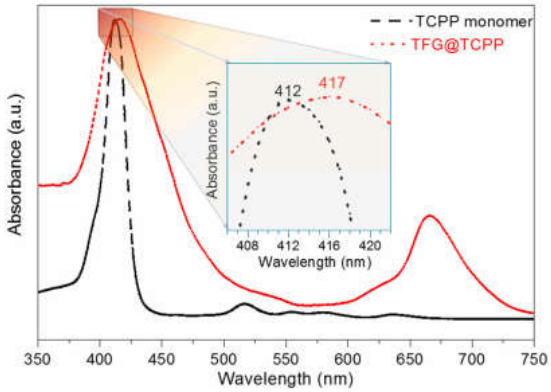

Figure 3.25. UV-VIS diffuse reflectance spectra of TCPP monomers and graphene/Fe_2O_3-TiO_2/TCPP

3.2. Evaluation of photocatalytic properties of synthesized porphyrin nanomaterials

3.2.1. Photocatalytic ability of the material (nano TCPP) to decompose RhB

The photocatalytic degradation of RhB pollutant under simulated sunlight irradiation using xenon lamp (350W) was studied to evaluate the photocatalytic efficiency of self-assembled TCPP nanofibers and TCPP monomers (Figure 3.26).

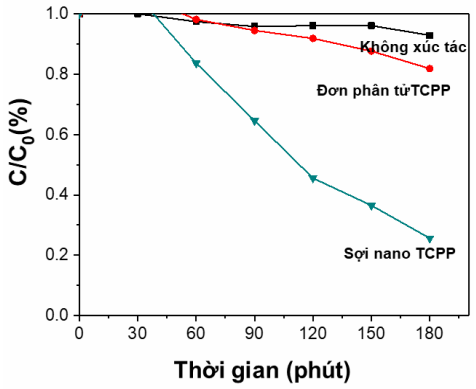

Figure 3.26. Catalytic efficiency for RhB under non-catalytic conditions and using different types of catalysts

The reusability of the self-assembled TCPP nanostructure as a photocatalyst for RhB removal was evaluated in an experiment under simulated visible light irradiation shown in Figure 3.27.

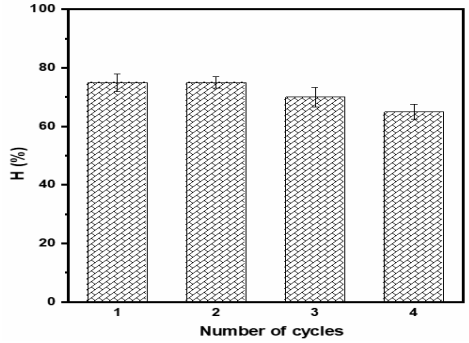

Figure 3.27. Reusability of TCPP nanofibers as photocatalyst for RhB removal after 4 cycles x 180 min/cycle

3.2.2. Photocatalytic ability of the material (Nano TTPAP) to decompose RhB

The photodegradation of RhB under simulated solar light irradiation using a xenon lamp (350 W) was used to investigate the photocatalytic performance of TTPAP aggregates compared with TTPAP monomer. Figure 3.28 shows the percentage of RhB removal versus time plot when TTPAP monomer and TTPAP aggregates were used as photocatalysts for the degradation of RhB under simulated visible light irradiation.

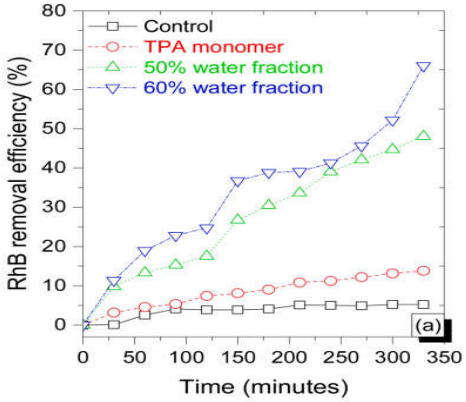

Figure 3.28. RhB degradation efficiency without using photocatalyst and with using photocatalyst fabricated by self-assembly of TTPAP molecules with different water contents

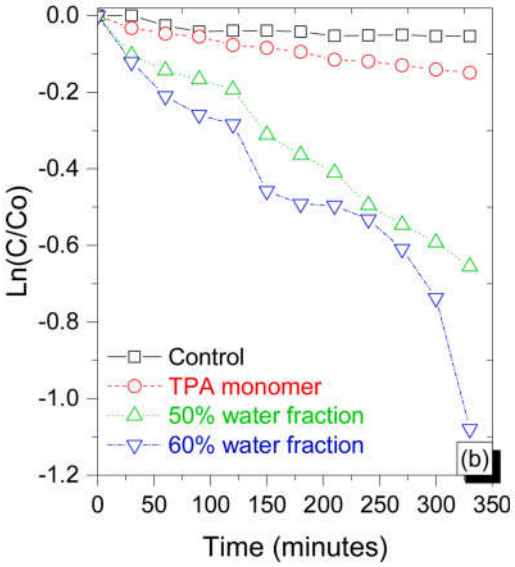

Figure 3.29. Simulation curve of TTPAP photocatalytic performance kinetics for RhB degradation

The degradation kinetics for RhB removal by TTPAP photocatalyst in aqueous solution were investigated by plotting $\ln(C/C_o)$ versus time (where C is the RhB concentration at time t and C_o is the initial RhB concentration), as shown in Figure 3.29.

The reusability of the self-assembled TTPAP nanostructure as a photocatalyst for RhB removal was evaluated in an experiment under visible light irradiation (Figure 3.30).

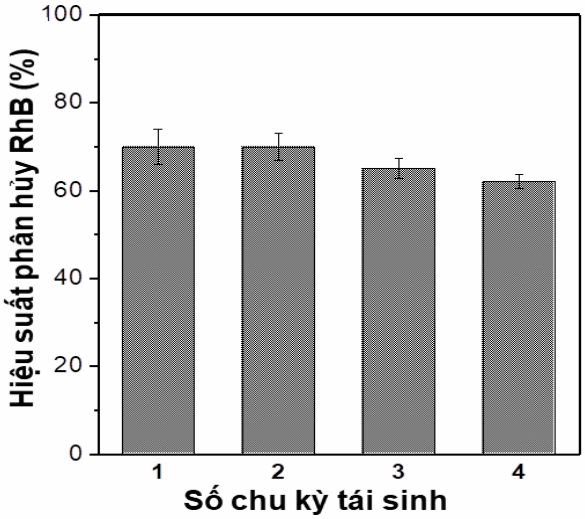

Figure 3.30. Reusability of TTPAP aggregates as photocatalysts for RhB removal after 04 cycles x 360 min/cycle.

3.2.3. Photocatalytic ability of materials to decompose RhB (Nano TTOP)

To evaluate the catalytic activity of the composites, a photocatalytic degradation test of RhB of TTOP monolayer and self-assembled TTOP nanocomposites was conducted under simulated sunlight irradiation conditions.

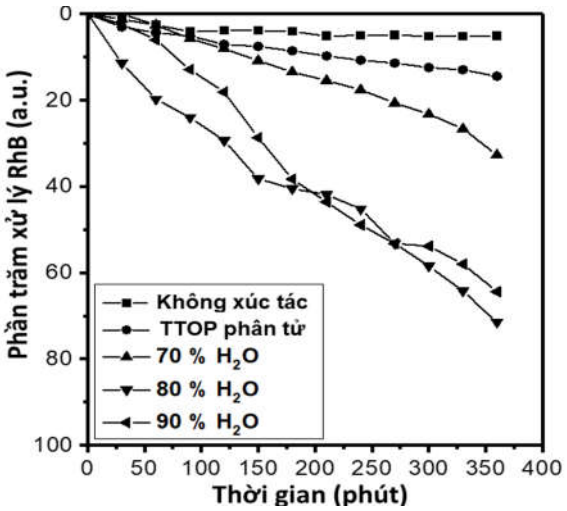

Figure 3.31. RhB degradation efficiency under non-catalytic conditions and using different types of self-assembled TTOP catalysts over time

The reusability of the self-assembled TTOP nanostructure as a photocatalyst for RhB removal was evaluated in the experiment under visible light simulation conditions shown in Figure 3.32.

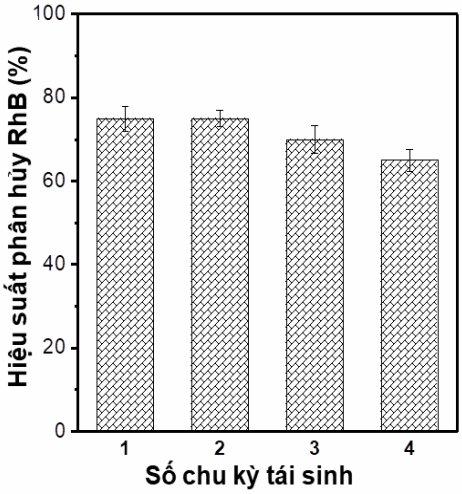

Figure 3.32. Reusability of the assembled TTOP nanostructure with 90% water content as a photocatalyst for RhB dye removal after 4 cycles x 360 min/cycle

3.2.4. Comparison of photocatalytic ability of nanomaterials TCPP, TTPAP and TTOP to degrade RhB

From the results of evaluating the photocatalytic efficiency of the nanostructured materials TCPP, TTPAP, and TTOP fabricated by the self-assembly method for the RhB decomposition process under the same conditions of the photocatalytic experiment (same initial RhB concentration and same illumination conditions), it was found that the nanostructured material TCPP was capable of decomposing up to 80% of RhB after 180 minutes, while RhB was only decomposed about 45% for the self-assembled TTOP catalyst and about 41% for the self-assembled TTPAP catalyst used as the photocatalyst.

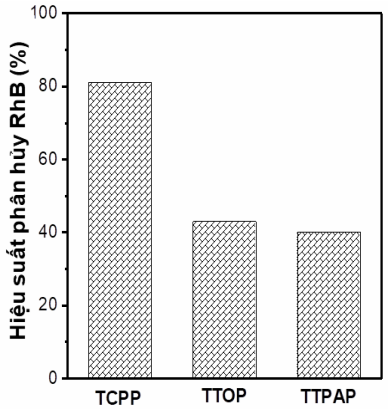

Figure 3.33. Comparison of RhB degradation efficiency of TCPP, TTOP and TTPAP under the same experimental conditions

3.3. Study on photocatalytic ability of RhB decomposition of TiO_2/TCPP material

Evaluation of the photocatalytic performance of TiO_2/TCPP composite compared with free-standing TiO_2 nanoparticles and TCPP nanofibers for the degradation of RhB dye under sunlight.

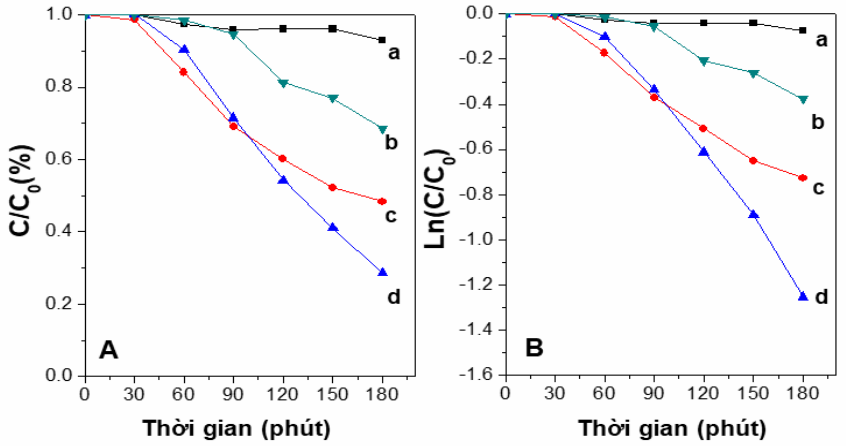

Figure 3.34. Photocatalytic degradation efficiency of RhB by (a) no photocatalyst, (b) TiO_2, (c) TiO_2 nanofibers, and (d) TiO_2/TCPP

The stability and reusability of the hybrid material for the degradation of RhB on TiO_2/TCPP hybrid material under simulated visible light irradiation were repeatedly conducted.

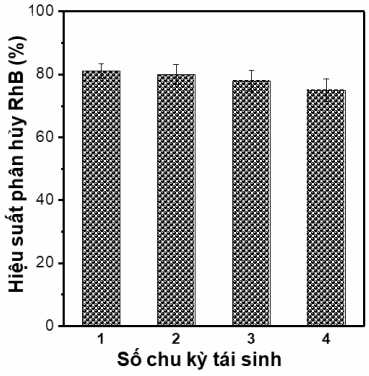

Figure 3.35. Reusability of TiO_2/TCPP photocatalyst for RhB dye degradation after 4 cycles x 180 min/cycle

3.4. Study on photocatalytic ability of RhB decomposition material (TFG@TCPP)

The photocatalytic activities of single porphyrin, graphene/Fe_2O_3-TiO_2 composite, TiO_2, porphyrin aggregates and Fe_2O_3-TiO_2@porphyrin hybrid materials against Rhodamine B are shown in Figure 3.36.

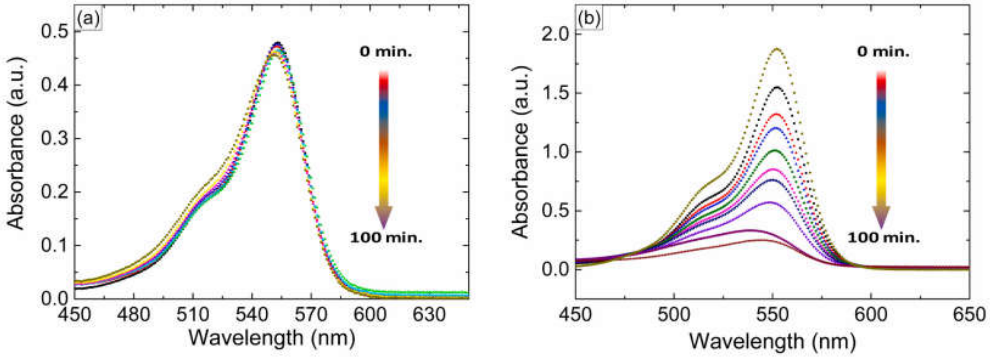

Figure 3.36. Photocatalytic performance for RhB degradation of (a) single TCPP and (b) graphene/Fe_2O_3-TiO_2/TCPP hybrid material over time

Illustrated in Figure 3.37a is the graph of the percentage decrease in RhB concentration over time and Figure 3.37b is the kinetic plot ln (A_t/A_0) of the photocatalytic reaction versus time, where Ao is the initial intensity of the peak and At is the intensity of the peak at time t.

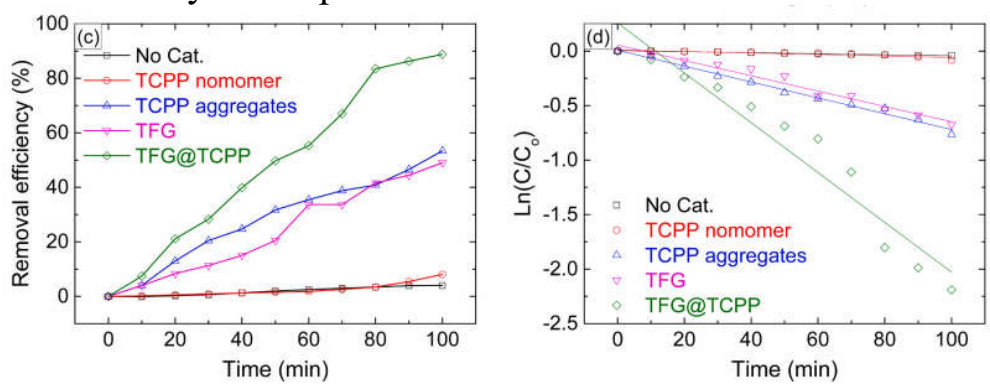

Figure 3.37. Plot of RhB concentration percentage reduction (a) and kinetic simulation curve (b) against time

The stability and reusability of the hybrid material for the degradation of RhB on graphene/Fe_2O_3-TiO_2/TCPP hybrid material under visible light irradiation were repeatedly investigated.

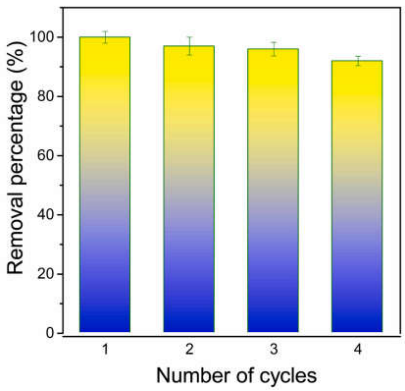

Figure 3.38. Regeneration ability of graphene@TiO_2-Fe_2O_3@TCPP in photodegradation of RhB.

3.5. Proposed photocatalytic reaction mechanism

To investigate the photocatalytic mechanism of porphyrin-based photocatalytic materials, the researcher first evaluated the mineralization ability and identified the primary free radicals involved in the degradation of organic dyes using porphyrin-based photocatalysts. The experiment was conducted using TCPP nanofibers as a typical representative photocatalytic material. Total carbon content (TOC) is an important index used to evaluate the degree of mineralization of aromatic molecules.

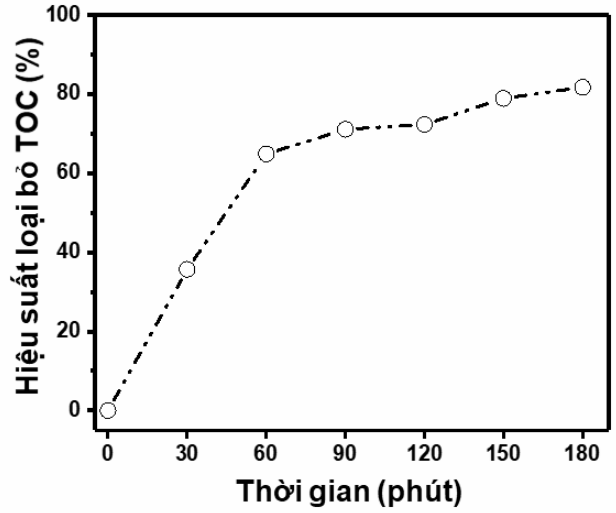

Figure 3.39. TOC removal efficiency during RhB photodegradation over time by TCPP nanofibers

The results shown in Figure 3.39 show that TOC decreased with reaction time and the TOC removal efficiency reached 82% after 180 minutes when using TCPP nanofibers as photocatalyst. The results in Figure 3.40 show that the presence of O_2^{-*} and $^*OH$ radical scavengers (BQ and IPA, respectively) significantly reduced the RhB degradation efficiency, from 80.12% to 16 and 11%, respectively.

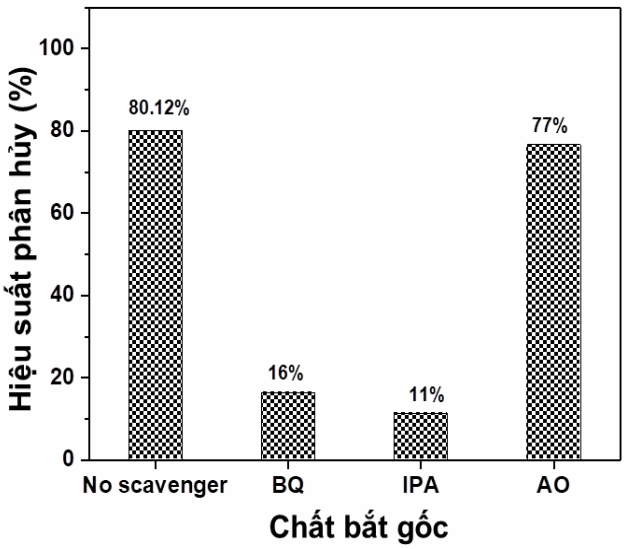

Figure 3.40. The influence of free radical scavengers on the RhB degradation efficiency of TCPP nanofiber materials

3.5.1. Proposed photocatalytic reaction mechanism for RhB decomposition of materials (Nano TCPP, TTPAP, TTOP)

Porphyrin derivatives, the structure and photochemical properties of nanostructured porphyrins similar to natural chlorophyll, have been studied as photosensitizers that enhance the efficiency of light energy absorption.

The photocatalytic mechanism for different porphyrin derivatives has been investigated and discussed. Therefore, based on the above results and discussions, a possible mechanism for the photocatalyst to work in the degradation of RhB dye is proposed (Figure 3.38).

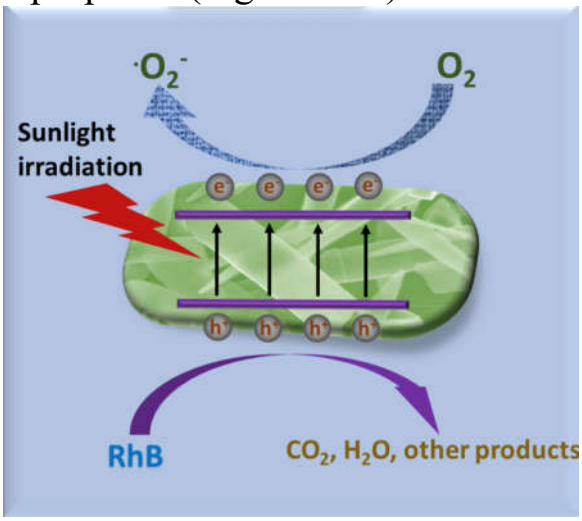

Figure 3.41. Photocatalytic reaction mechanism of RhB degradation of self-assembled TCPP, TTPAP, TTOP under simulated sunlight radiation

3.5.2. Proposed photocatalytic reaction mechanism for RhB degradation of the material (TiO_2/TCPP)

Based on the above results and discussions, a plausible mechanism for the enhanced photocatalytic activity of the TiO_2/TCPP nanofiber hybrid material is proposed as shown in Figure 3.42.

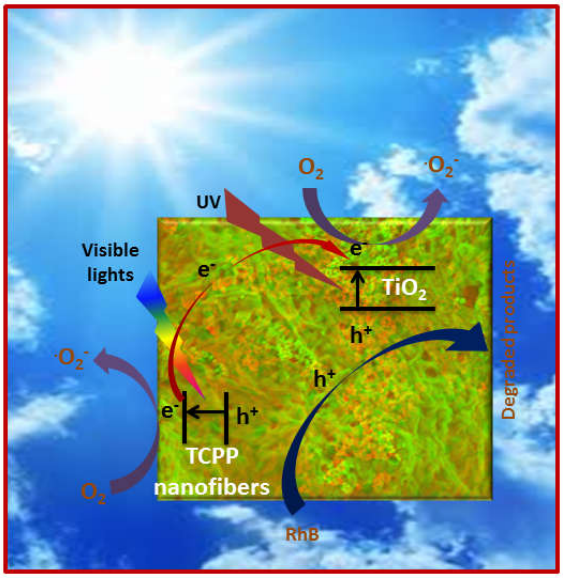

Figure 3.42. Photocatalytic reaction mechanism of RhB degradation of TiO_2/TCPP nanohybrid material under simulated sunlight irradiation

3.5.3. Proposed photocatalytic reaction mechanism for RhB degradation of the material (TFG@TCPP)

Based on the literature and results presented above, the photocatalytic mechanism of graphene@Fe2O3-TiO2@porphyrin hybrid material is shown in Figure 3.43.

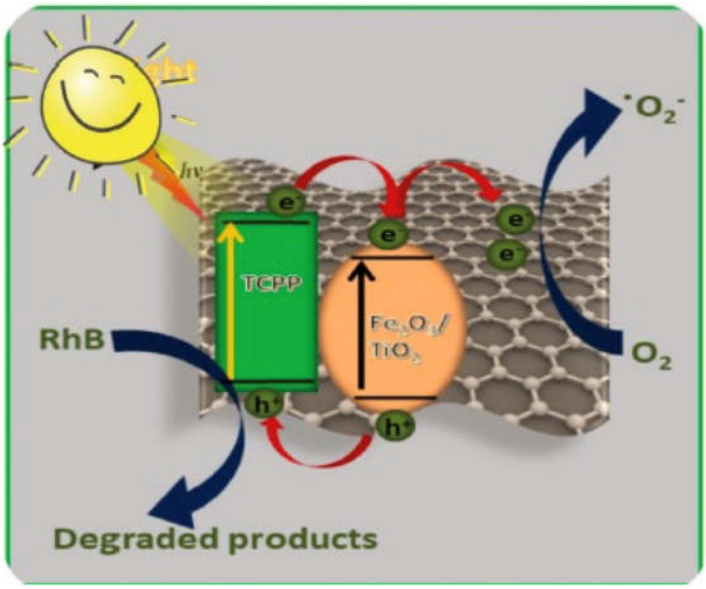

Figure 3.43. Mechanism of graphene/Fe_2O_3-TiO_2@porphyrin photocatalyst for photodegradation of RhB

CONCLUSION

1. Pioneering the field, we have successfully synthesized nanostructured materials using a self-assembly method from three porphyrin derivatives. These include: tetrakis-triphenylamineporphyrin (TTPAP); 5,10,15,20-tetra (3,4,5-trimethoxyphenyl) porphyrin (TTOP) and 4,4,4,4 -((Porphin- 5,10,15,20-tetrayl) tetrakis benzoic acid (TCPP). The self-assembled TCPP porphyrin nanofibers have a nanofiber structure with a diameter of 20-30 nm and a length of several microns. The TTPAP porphyrin nanofibers are assembled into a rod-like microstructure with a length of about 5μm and a diameter of 0.5 - 1.5 μm. The self-assembled TTOP porphyrin nanofibers have several different morphologies such as rods, spheres, and sheets. The photocatalytic ability of the fabricated porphyrin nanomaterials was evaluated. The results showed that TCPP nanofibers have higher photocatalytic efficiency than the nanostructured materials of TTPAP and TTOP.
2. We have achieved a significant milestone with the successful fabrication of nanofiber hybrid materials TiO2/TCPP by self-assembly method. The fabricated material demonstrates that TiO2 still retains the granular nanostructure and is well integrated into the TCPP nanofiber network with a width of about 100 nm and a length of several micrometers. The TiO2/TCPP hybrid material showcases an impressive high photocatalytic efficiency for RhB dye.
3. The graphene/Fe2O3-TiO2/TCPP nanofiber hybrid material has been successfully fabricated by self-assembly. The fabricated material has a high photocatalytic ability for dye and a decomposition rate of 1.12 x 10-2/min.
4. Based on the experimental results and previously published works, the photocatalytic mechanism of the fabricated materials in the decomposition of Rhodamine B under simulated sunlight conditions has been initially demonstrated. The increased catalytic efficiency of the material systems in the thesis is due to the increased ability to absorb light energy in the visible spectrum, the reduced recombination ability of electron/hole pairs, and the photocatalytic effect of different semiconductors.

NEW CONTRIBUTIONS OF THE THESIS

1. Successfully fabricated nanostructured materials from some new porphyrin derivatives (TCPP, TTPAP, and TTOP) by the self-assembly method with the potential to be used as photocatalytic materials in the treatment of Rhodamine B degradation in aqueous environments.
2. Successfully fabricated TiO2/TCPP nanohybrid materials by the self-assembly method with high photocatalytic activity for Rhodamine B degradation in aqueous environments under conditions simulating sunlight.
3. Successfully fabricated graphene/Fe2O3-TiO2/TCPP nanohybrid materials by self-assembly method with good photocatalytic activity for Rhodamine B degradation in aqueous environments under conditions simulating sunlight.

DANH MỤC CÁC CÔNG TRÌNH ĐÃ CÔNG BỐ CỦA LUẬN ÁN

[1] **Duong Duc La,** ***Tuan Anh Nguyen****,* X. Sang Nguyen, Tuan N. Truong, H. Phuong Nguyen T., Ha D. Ninh, H. Tung Vo, Sheshanath V. Bhosale, S. Woong Chang, Eldon R. Rene, Tran Hung Nguyen, Sang Moon Lee, **Lam D. Tran***, D. Duc Nguyen**, 2021, Self-assembly of porphyrin on the surface of a novel composite high performance photocatalyst for the degradation of organic dye from water: Characterization and performance evaluation, *Journal of Environmental Chemical Engineering*, 9, 106034.

[2] **D. Duong La,** Ratan W. Jadha, Nilesh M. Gosavi, Eldon R. Rene, ***Tuan Anh Nguyen****,* Bui Xuan-Thanh, D. Duc Nguyen*, W. Jin Chung, S. Woong Chang, X. Hoan Nguyen, **Lam Dai Tran,** Sheshanath V. Bhosale*, 2021, Nature-inspired organic semiconductor via solvophobic self-assembly of porphyrin derivative as an effective photocatalyst for degradation of rhodamine B dye, *Journal of Water Process Engineering*, 40, 101876.

[3] ***Nguyễn Tuấn Anh****,* Lê Đình Khiêm, Trần Thị Như Quỳnh, Trương Ngọc Tuấn, Ninh Đức Hà, Nguyễn Thị Hoài Phương, Nguyễn Thị Hồng Phượng, **Trần Đại Lâm, Lã Đức Dương***, 2021, Nghiên cứu ảnh hưởng của hàm nước đến quá trình hình thành cấu trúc nano porphyrin bằng phương pháp self-assembly và hiệu quả xúc tác quang đối với xử lý phẩm màu, *Tạp chí xúc tác và hấp phụ Việt Nam*, 10 - issue 3, 47-51.

[4] Trần Văn Chinh, ***Nguyễn Tuấn Anh****,* Nguyễn Thị Hoài Phương, Mai Hữu Thuấn, Trần Văn Khanh, Đinh Thế Dũng, Nguyễn Thị Hồng Phượng, **Trần Đại Lâm, Lã Đức Dương***, 2020, Nghiên cứu chế tạo vật liệu copper ferrite biến tính với porphyrin ứng dụng làm xúc tác quang cho xử lý phẩm màu MB trong nước, *Tạp chí Xúc tác và hấp phụ Việt Nam*, 9 - issue 3, 107-111.